Final Report

1. **DOE Award #:** DE-FG02-07ER46389
   Award Institution: Miami University, Wright State University (subaward)
2. **Project Title:** Defect Chemistry Study of Nitrogen Doped ZnO Thin Films
3. **Report covering period**: June 1st, 2007-May 30th, 2010
4. **Accomplishment**

In the past 2-1/2 years, under a DOE grant, our team has investigated the defect chemistry of ZnO:N and developed a thermal evaporation (vapor-phase) method to synthesis *p*-type ZnO:N. These investigations have resulted in **one** published M.S. student thesis, **eight** published papers in Optical Materials (1), Electronic Materials Letters (1), Chemical Physics Letters (1), Journal of Applied Physics (1), Applied Physics Letters (2), J. Vac. Sci. and Tech. B (2).

Each subtitle is followed by the publications generated during the past DOE effort:

(1) P-type Nitrogen Doped ZnO Films Grown By Thermal Evaporation
"Enhanced p-type Conductivity of Nitrogen Doped ZnO via Nano/Micro Structured rods and Zn-rich Co-doping Process" Electronic Materials Letters, Vol. **7** No. 2 pp.115-119, 2011.

Two different N dopant precursors, pure NO and 5% NO/N_2 mixture, and two processes are used to investigate the controversial issue of single atom N and diatom N_2 effect on film conductivity. This study showed that the effectiveness of dopant precursor is process dependent.

ZnO is a naturally n-type material, mainly due to donor-type impurities such as Al, but also partially due to native defects, in particular, the zinc interstitial [1-2]. Thus, theoretically, if such impurities and defects could be eliminated, and if acceptors such as N could be incorporated, then a high hole concentration would be possible. In this study, two separate processes of thermal evaporation deposition were designed to determine the effects of oxygen nonstoichiometry.

Process I contained two steps. In the first step, a ZnO film was formed by thermal evaporation of Zn powder in oxygen ambient at 500°C for 2 hrs. In the second step, the as-grown ZnO film was annealed in nitrogen gas for an hour to form ZnO:N. Two nitrogen precursors and annealing temperatures were investigated.

Process II contained three steps. The first step and the third step were the same as those of process I. However, a second step was added, namely, a saturated-O_2 anneal of the as-grown ZnO from the 1^{st} step. The idea here was to eliminate O vacancies, which are donors and will compensate acceptors such as N_O.

Hall-effect measurements were performed at room temperature in the van der Pauw configuration, with an Accent 5500 apparatus. Photoluminescence measurements were performed at 4.2 K, and excitation, dispersion, and detection were accomplished, respectively, with a 45-mW HeCd laser, a Spex 1269 1.26-m spectrometer, and a photomultiplier detector. Resolution was better than 0.01 meV in the spectral range important for this study. X-ray diffraction (XRD) was used to characterize the crystal structure of the ZnO films. Scanning Electron Microscopy (SEM) and Energy Dispersive X-ray (EDX) were used to obtain the surface morphology and element composition of the film, respectively.

The Hall-effect measurements in Table 1 indicate that annealing ZnO film in 5% NO/N_2 is a feasible method of synthesizing *p*-type ZnO:N. Each sample was run at least twice, and at different currents, to validate the electrical properties. When *p*-type conductivity was measured in both runs, it was recorded as *p*-type. When both runs indicated *n*-type, it was recorded as *n*-type. When one run indicated *p*-type and the other indicated *n*-type, it was recorded as *mixed*-type. The conductivity of the film depended not only on the dopant gas but also on the growth process. For example, under a 350 °C anneal, the ZnO:N film annealed in 5% NO/N_2 mixture exhibited *p*-type behavior by process I but *n*-type behavior by process II. When increasing the annealing temperature to 400 °C, both Process I and II produced *n*-type films for 5% NO/N_2 dopant gas. On the other hand, for the films annealed in pure NO, n-type films were generated at 350 °C and mixed-type films at 400 °C, for both processes. This indicates that N_2 plays a critical role during the annealing process. The common belief that pure NO is better than 5% NO/N_2 for producing p-type ZnO is evidently not correct in every situation.

Table 1. Hall-effect measurements of ZnO:N
P: Process. AT: Annealing temperature (°C).

Annealing Gas	P	AT	type	Resis	Mob	Carrier concentration
				Ω·cm	cm^2/V-s	per cm^3
ZnO	-	-	n	$1.08x10^2$	0.519	1.11×10^{17}
Pure O_2	II	500	n	$4.35x10^3$	0.914	1.57×10^{15}
5% NO/N_2	I	350	p	$1.58x10^1$	2.47	1.60×10^{17}
5% NO/N_2	II	350	n	$4.96x10^1$	2.72	4.62×10^{16}
5% NO/N_2	I	400	n	$3.83x10^1$	1.57	1.04×10^{17}
5% NO/N_2	II	400	n	$2.81x10^2$	0.797	$2.79x10^{16}$
Pure NO	I	350	n	$6.57x10^1$	1.07	8.85×10^{16}
Pure NO	II	350	n	$7.19x10^2$	0.827	1.05×10^{16}
Pure NO	I	400	mixed	$2.42x10^3$	-	-
Pure NO	II	400	mixed	$1.15x10^3$	-	-

The EDX has indicated that the as-grown ZnO contains excess Zn existing at the film surface, perhaps mostly at the tips of the nanorods shown in Fig. 1(a). The Zn/O atomic ratio of the as-grown ZnO film is 3:1 at the surface, which proves the existence of excess Zn at the surface of the as-grown film. The excess Zn might be deposited onto the ZnO rods by the Zn vapor during the cooling. These sharp tips shown in Fig. 1(a) disappeared or became dull after annealing in O_2 or in any dopant gas (Fig. 1(b)) and the EDX showed that after annealing, the Zn/O atomic ratio was reduced to 3:4 at the film surface. The ZnO film thickness is about 200 nm.

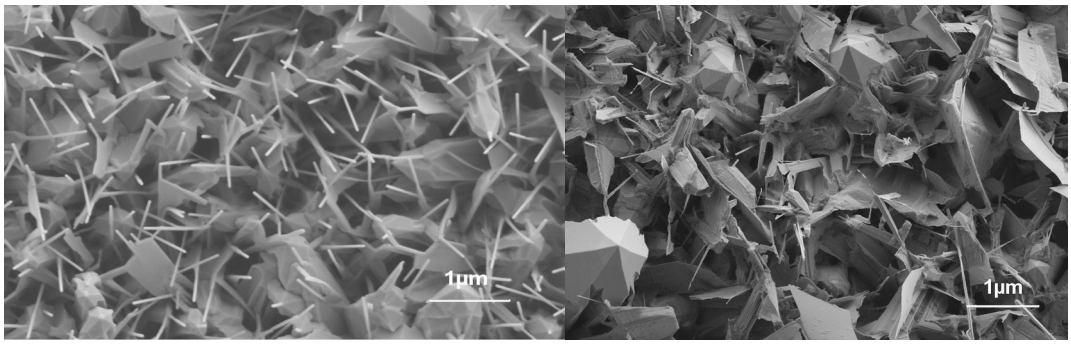

Fig. 1(a) As-grown ZnO (left) (b) ZnO after annealing (right)

The possible chemical reactions involved in the growth and annealing processes are presented in Table 2. The *p*-type conductivity of the films annealed in 5% NO/N_2 in Process I is attributed to the formation of Zn_3N_2 due to the presence of N_2 in the 5% NO/N_2 mixture by reaction 3 (R3). The formation of Zn_3N_2 helps to capture the N_2 in the 5% NO/N_2 and converts N_2 to form the Zn-N bond in Zn_3N_2. Zn_3N_2 further reacts with NO to form ZnO:N via reaction R4. In other words, reactions R3 and R4 enhance the nitrogen incorporation into the ZnO film.

Table 2. Possible reactions in Processes I and II
R: reaction

	Process I		Process II	
	5% NO/N_2	Pure NO	5% NO/N_2	Pure NO
Step 1	Zn (s) → Zn (g) (R1) $Zn + 1/2O_2 \rightarrow ZnO$ (R2)			
Step 2	-		$Zn + 1/2O_2 \rightarrow ZnO$ (R2) (Residual Zn reaction with oxygen)	
Step 3	$Zn + 1/3N_2 \rightarrow 1/3Zn_3N_2$ (R3) $Zn_3N_2+NO \rightarrow$ ZnO:N(R4) $ZnO + NO \rightarrow$ ZnO:N (R5)	$ZnO + NO \rightarrow$ ZnO:N (R5)	$ZnO + NO \rightarrow$ ZnO:N (R5)	

Reaction R4 is affected in two different ways when increasing temperature. At higher temperature the sticking coefficient of the NO in the 5% NO/N_2 gas is lower, thus inhibiting R4. On the other hand, all of the chemical reactions, including R4, are temperature dependent and usually are enhanced at higher temperatures. Apparently, 350°C is a critical temperature for the efficacy of 5%NO/N_2 in process I. At temperatures lower than 350°C, all of the films annealed in 5% NO/N_2 are *n*-type, evidently because the chemical reactivities of R3 and R4 are lower. At 350°C, the increased chemical reactivities of R3 and R4 produce *p*-type material. When further increasing the temperature to 400°C, *n*-type material is obtained due to the poor sticking coefficient of NO, which inhibits R4. When pure NO is used, the sticking coefficient does not play a significant role due to the oversaturation of NO. The film conductivity is thus determined by the temperature dependence of reaction R5. At 350°C, the films are n-type for both processes I and II, but then become of "mixed" type (indeterminate) at 400°C. In process II, films grown with 5%NO/N_2 are *n*-type at any temperature. This is because the excess Zn from the 1st step reacts with the pure O_2 in the 2nd step, via reaction R2, before the introduction of the nitrogen

dopant gas. Thus, the N_2 in the 5% NO/N_2 mixture does not have any excess Zn with which to react and form Zn_3N_2 and thus creates only n-type behavior at both 350°C and 400°C. Our previous EXFAS study [3] of process II indicated that the N_2 molecules will be trapped in the surface when there is no free Zn to react with and contribute to the $(N\text{-}N)_O$ donor defects.

Table 3 presents some of the photoluminescence properties. The interesting lines can be roughly grouped into seven regions: 1.9 eV (red band); 2.5 eV (green band); 3.31 eV (acceptor band); 3.33 – 3.35 eV (defect lines); 3.360 (Al/Ga lines); 3.362 eV (X lines); and 3.366 eV (surface band). The 3.31-eV band was first seen in *p*-type material [7] and has been observed many times since [4]. Although there is wide disagreement as to the detailed nature of the transition, almost all workers believe that an acceptor is involved. The 3.33 – 3.35-eV lines can have one to five or even more components, depending on the growth process, and since some of these are produced by electron irradiation, they are designated “defect lines” in this work [5]. The sharp lines near 3.360 eV are mainly donor-bound excitons due to Al and Ga, although a defect-related line is also known to exist in this region [5]. The 3.362-eV line is also a donor-bound-exciton transition, but its origin is unknown. Finally, a 3.366-eV band, similar to ours, has been shown to be surface-related [6]. From the results listed in Table 3, the relative strengths of the acceptor band seem to be correlated with the presence of N, except for the sample annealed only in O_2 at 500 °C. We can explain this result as follows: the as-grown ZnO has excess Zn at the film surface as described earlier. Upon annealing in pure O_2, most of the excess Zn will react with O_2 but some of the Zn atoms will diffuse into the bulk, attaching themselves to various types of acceptors. One such Zn_I-acceptor complex which has been proposed is $Zn_I\text{-}N_O$ [5], and even though the sample in question has not been annealed in N, still it likely contains N, a very common background impurity in ZnO.

Table 3. Photoluminence of ZnO:N

P: Process; AT: Annealing temperature (°C); CT: Conductivity type.

Annealing Gas	P	AT	CT	Rank of NBE intensities (1: Strongest)			3.33–3.35 eV (defect lines)	3.31 eV (acceptor band)
				3.360 eV	3.362 eV	3.366 eV		
ZnO	-	-	n	3	1	2	Very weak	Very weak
Pure O_2	II	500	n	3	2	1	Strong	strong
5% NO/N_2	I	350	p	3	2	1	Very weak	Strong
5% NO/N_2	II	350	n	3	2	1	Very weak	Strong
5% NO/N_2	I	400	n	3	1	2	Very weak	Strong
5% NO/N_2	II	400	n	3	2	1	Medium	Strong
Pure NO	I	350	n	3	1	2	Weak	Strong
Pure NO	II	350	n	3	2	1	Strong	Strong
Pure NO	I	400	mixed	3	1	2	weak	Strong
Pure NO	II	400	mixed	3	1	2	medium	Strong

P-type, nitrogen-doped, ZnO films were formed, for the first time, by thermal evaporation. It was shown that the film conductivity depends not only on the dopant gas but also on the growth and annealing process. The formation of Zn_2N_3 and its further reaction with NO are thought to be important elements in this process. If so, the use of Zn_2N_3 as a starting material might further enhance nitrogen incorporation into the films. Correlations were obtained between

electrical and optical properties, so that the latter can serve as useful tools in the development of better p-type ZnO.

References for this paper:

[1] H.S. Kim, E.S. Jung, W.J. Lee, J.H. Kim,S.O. Ryu, S.Y. Choi, Ceram. Int. **34**, 1097 (2008)
[2] Y. Natsume, H. Sakata, Mater. Chem. Phys. **78**, 170 (2002)
[3] W. Mu, L. Kerr, N. Leyarovska, Chem. Phys. Lett. **469,** 318 (2009)
[4] D.C. Look, B. Claflin, Ya. I. Alivov, and S.J. Park, phys. Stat. sol. (a) **201**, 2203 (2004)
[5] D.C. Look, G.C. Farlow, P. Reunchan, S. Limpijumnong, S.B. Zhang, and K. Nordlund, Phys. Rev. Lett. **95**, 225502 (2005)
[6] L. Wischmeier, T. Voss, I. Rückmann, J. Gutowski, A.C. Mofor, A. Bakin, and A. Waag, Phys. Rev. B **74**, 195333 (2006)
[7] D.C. Look, D.C. Reynolds, C.W. Litton, R.L. Jones, D.B. Eason, G. Cantwell, Appl. Phys. Lett. **81**, 1830 (2002)

(2) Extended X-Ray Absorption Fine Structure Study of p-type Nitrogen Doped ZnO

- "Extended X-Ray Absorption Fine Structure Study of p-type Nitrogen Doped ZnO," Chemical Physics Letters, Vol. 469, pp 318-320, 2009.

The doping mechanism and the crystal structure parameters are very important but are unknown in the development of *p*-type ZnO:N. In this study, the EXAFS study was performed on ZnO:N grown on glass substrates in our tube furnace reactor using NO or NO/N_2 as dopant source using process II described earlier which are the commonly used growth conditions.

The X-ray absorption coefficient (μ) shown in Fig. 2 was acquired from the pure ZnO (without annealing in dopant gas) near the Zn *K* edge measured at room temperature. Fig. 3 shows the calculated EXAFS of pure ZnO and p-type ZnO at the Zn *K* edge as a function of the photoelectron wave vector *k*. Processed by Fourier transformation and the theoretical calculation, the EXAFS data were converted to R space (radius from Zn atom) as shown in Fig. 4. As seen from Fig. 4, the Zn–Zn bonding is located at peak position of 3.22 Å. The broad peak around 1.9 Å is due to Zn–O. Nitrogen doping seems to affect the two shoulder peaks of Zn–O peak. The shoulder peaks at 1.00 Å (marked *) and 1.15 Å (marked Δ) were less significant for undoped ZnO (Fig. 4a) than these for the ZnO:N (Fig. 4b and c). These two shoulder peaks are more prominent in the film with better p-type performance (ZnO:N using pure NO as dopant gas, Fig. 8b). Table 1 shows the bonding length of Zn–O and Zn–Zn as derived from EXAFS. The pure ZnO film has Zn–Zn and Zn–O bonding length of 3.213 Å and 1.927 Å, respectively. This is in good agreement with the bonding length as obtained from x-ray diffraction (XRD) study (Zn–O 3.254 Å and Zn–Zn 1.979 Å) shown in Fig. 5.

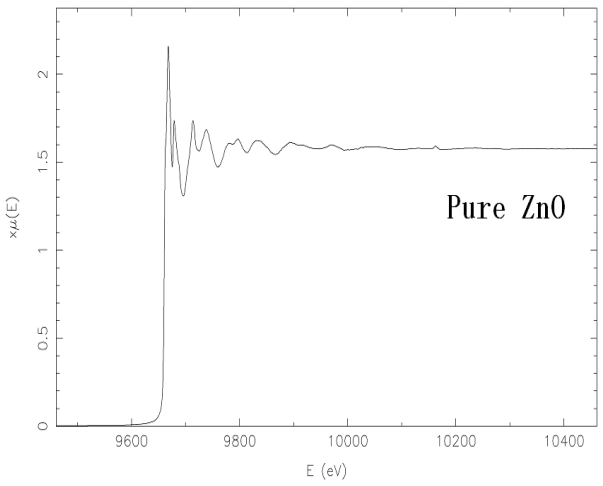

Fig. 2. Normalized x-ray absorption coefficient of pure ZnO as a function of incident x-ray energy at the Zn K edge.

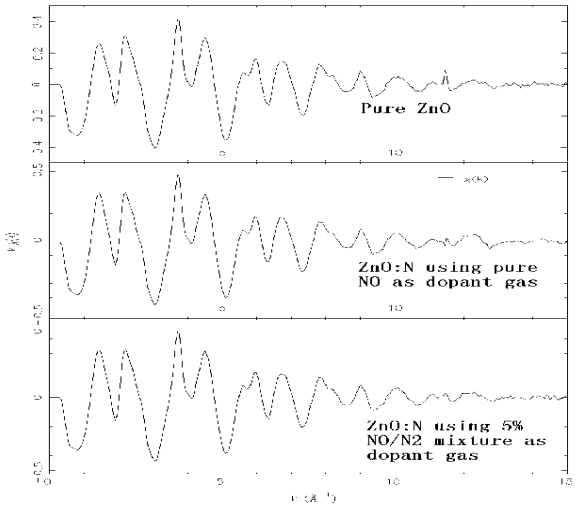

Fig 3. EXAFS ($\chi^2\kappa$) from ZnO film (top), ZnO film annealed in pure NO (middle) and ZnO film annealed in 5% NO/N_2 mixture (bottom) as a function of the photoelectron wave vector *k*.

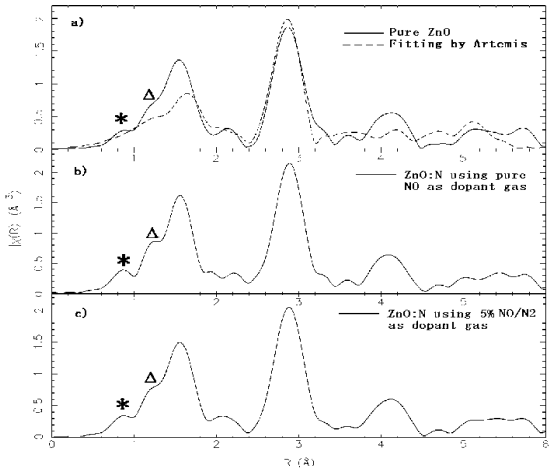

Fig. 4: Fourier transformed EXAFS data. a) ZnO film & Artemis fitting, b) ZnO film annealed under pure NO and c) ZnO annealed under 5% NO/Nitrogen mixture

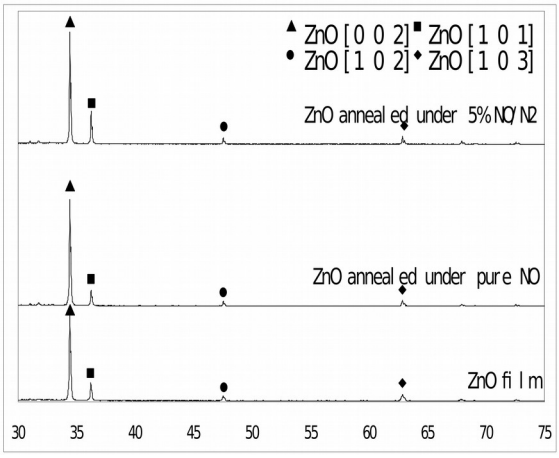

Fig. 5. XRD of ZnO film, ZnO film annealed in pure NO (middle) and ZnO film annealed in 5% NO/N2 mixture

As shown in Table 4, the bonding length of ZnO obtained from EXAFS experiment fits well to the values calculated by Artemis. The bonding lengths of Zn–O and Zn–Zn were increased after annealing for both nitrogen dopant gases. The increase of Zn–Zn bonding length might be due to the steric effect. In a wurtzite structured ZnO unit cell, one oxygen atom is neighboring with four Zn atoms forming the geometry of triangular pyramid with oxygen located in the pyramid center. The substitute of N–N diatom occupies larger space than a single oxygen atom. The Zn atoms will then be pushed away from their original sites and thus enlarge the distance between Zn–Zn. The high electron density of the N–N will also repulse the electron pair between Zn–N to be shifted to the Zn atom side, which causes the Zn atoms to be withdrew outwards. Since the Zn–N

bonding (1.77 Å) is actually shorter than Zn–O bonding (1.939 Å), The increase of Zn–O bonding length from EXAFS data might indicate that during the annealing process, nitrogen atom can exist in the form of diatom N–N in ZnO film. The extra N_2 molecules in the 5% NO/N_2 gas lowered electrical performance as revealed by the higher resistivity and lower hole concentration. It has been well reported in the literature that N–N acts as a donor in ZnO:N film. In conclusion, ZnO:N crystal fine structure formed by process I was analyzed by EXAFS. It has been shown from the EXAFS data that the bonding length of Zn-Zn and Zn-O of p-type ZnO:N is longer than these of n-type ZnO. It indicates that N atom is not simply substituting the O atom. There could be the existence of N-N bonding. A reduction of the p-type performance was observed for ZnO:N using 5% NO/N_2 which is probably due to the presence of more diatom N-N in the film.

Table 4: ZnO and ZnO:N Bonding length and their electrical property.

	Zn-O d(Å)	Zn-Zn d(Å)	Resistivity ρ (Ω·cm)	Mobility $cm^2/V\text{-}S$	Carrier Conc. $/cm^3$	Conductivity type
ZnO Model calculated by Artemis	2.04	3.229	-	-	-	-
ZnO film	1.927	3.213	3.23	5.30	3.65×10^{17}	n
ZnO:N using dopant gas of pure NO	1.96	3.236	2.56×10^{1}	0.614	3.96×10^{17}	p
ZnO:N using dopant gas of 5% NO/N_2 mixture	1.964	3.243	3.24×10^{2}	7.45	2.58×10^{15}	p

(3) Hall, PL and DLTS studies

- D.C. Look, "Two-Layer Hall-Effect Model With Arbitrary Surface-Donor Profiles Application To Zno", J. of Applied Physics, Vol. 104, 063718, 2008.
- D.C. Look, B. Claflin, and H.E. Smith, "Origin of Conductive Layer In Annealed ZnO", Appl. Phys. Lett. 92, 122108, 2008.
- Z. Yang, D.C. Look, and J.L. Liu, "Ga-Related Photoluminescence Lines In Ga-Doped Zno Grown By Plasma-Assisted Molecular-Beam Epitaxy", Appl. Phys. Lett. 94, 072101, 2009.
- D.C. Look, G.C. Farlow, F. Yaqoob, L.H. Vanamurthy, and M. Huang, "In-implanted ZnO: Controlled Degenerate Surface Layer", J. Vac. Sci. and Tech. B, accepted. 2009
- Z-Q. Fang, B. Claflin, D.C. Look, Y-F. Dong, and L. Brillson, "Metal Contacts on Bulk Zno Crystal Treated With Remote Oxygen Plasma", J. Vac. Sci. and Tech B, 27, 1774 (2009).

The present DOE project is based on ZnO thin films and nanostructured layers, both of which have high surface/volume ratios and thus require a detailed understanding of ZnO surfaces. We have conducted the Hall and PL studies to understand why ZnO samples so often have a thin, highly conductive n-type surface layer, which of course can be very detrimental to development of p-type material. Supported by DOE and other funding agencies, we have made the following conclusions and findings (1) Group-III donor-type elements, Al, Ga, and In, diffuse into the surface region during growth or annealing stages, and make the surface strongly n-type. Care must be taken to avoid this problem. (2) An improved algorithms to determine the electrical properties of these conductive surface layers, even when they are masked by the normal high conductivity in the bulk regions. These algorithms are being offered to the public free of charge. (3) Ga-related photoluminescence lines have appeared in almost every ZnO sample that we have measured, from any source. The reason for the omnipresence of Ga is that it is a common impurity in Zn-containing ores. The same is true of Al, and to a lesser extent, In, and the

diffusion of these elements is what caused the strong surface conductive layer. (4) The implantation of In can also create a highly conductive surface layer. This was a somewhat surprising result, because implantation in ZnO has seldom been successful as a doping technique. It is possible that implantation of acceptor-type elements, such as N, might also provide a way to obtain p-type ZnO. (5) The remote oxygen plasma treatments at room temperature plays important role on the formation of metal/ZnO Schottky contacts and electron traps, including surface electron traps, on two polarities of bulk vapor phase-grown ZnO. This study serves as reference for future DLTS study on p-type thin film ZnO. In last funding period, DLTS measurements were performed on a structure of N-doped p-type ZnO grown n-type Si by vapor phase technique, with annealed at 5 % NO, 350 C for 1 hr. The as-grown N-doped p-ZnO material shows many nanorods on the surface. The p-ZnO/n-Si p-n junction shows some rectification at RT, and very poor rectification at lower temperatures, and very small capacitance, which does not change with bias, probably due to presence of interface silicon dioxide. Thus, this is not a good p-n junction sample, suitable for DLTS measurements. However, we tried to run DLTS on the junction and got preliminary DLTS results, as shown in Fig. 6. From DLTS vs Tw (transient period, something like rate windows) measurements (see Fig. 6a), we do see that peak of hole traps (H2 with H1 on its rising shoulder) shifts with Tw, which confirms that they are real traps. While from DLTS vs t_P (forward filling pulse width) measurements (see Fig. 6b), we find increase of the peak height with t_P, which indicates that the traps are not due to isolated point defects, but probably associated with extended defects or nanorod feature. The peak position of H2/H1 is very close to the H4 (0.48 eV) mentioned above, which probably confirms presence of major hole traps in N-doped ZnO. Convincible DLTS study on as-grown and irradiated p-ZnO:N appears to be highly dependent on whether or not good ZnO/Si p-n junctions can be obtained. Therefore design and fabrication of good ZnO p-n junction (either hetero- or homo-structures) will be our task in the proposed project.

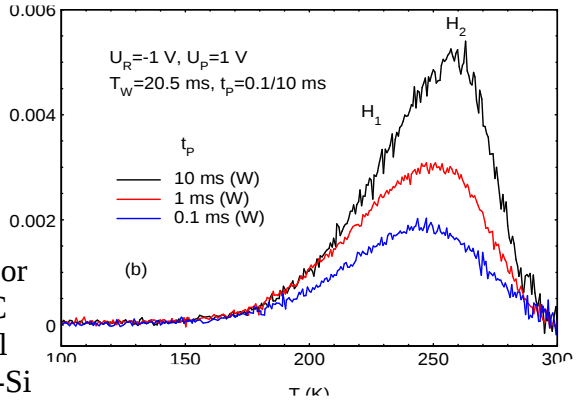

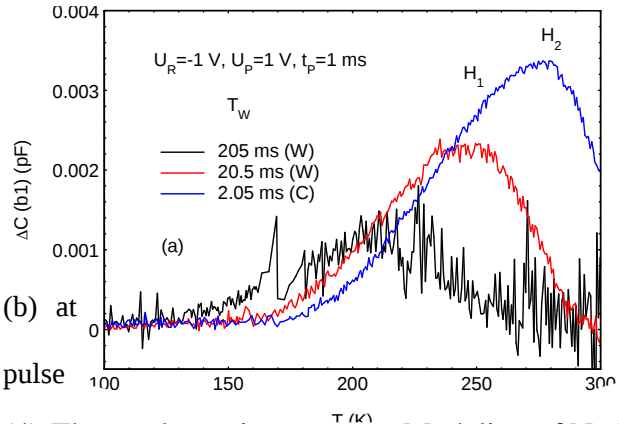

Fig. 6. DLTS spectra, measured mainly upon warming (a) at different transient periods (T_W's) and different forward filling pulse width (t_P's), on a p-ZnO:N/n-Si junction. Bias U_R=-1 V and filling pulse height U_P=1 V.

(b) at

(4) Thermodynamic Modeling of Native Defects in ZnO

- Accepted for publication in Optical Materials

In this paper, the undoped ZnO was taken as an example to introduce how to use this point defect model to interpret the intrinsic doping state determined by the microscopic equilibrium. The corresponding native defects are the Zn vacancy (Va_{Zn}), O vacancy (Va_O), antisite defects (Zn_O and O_{Zn}), interstitial Zn (Zn_i) and O (O_i) and their different ionized charge states. The selection of these defects into the model is because the defects of Va_{Zn}^{-2}, Va_O^{+2}, Zn_O^{+2}, Zn_i^{+2} and O_i^{-2} have relatively lower formation energies than other defects according to the first-principle calculations [1]. Thus, the model of undoped ZnO can be simplified as follows,

$$(Zn, Va_{Zn}^{-2})(O, Va_O^{+2}, Zn_O^{+2})(Va, Zn_i^{+2}, O_i^{-2})(Va, e^-, h^+)$$

Va_O, Zn_O and Zn_i are donors, and Va_{Zn} and O_i serve as acceptors. The equilibrium concentrations of these defects determine the conductivity type at different equilibrium conditions.

It is worth to note here that there has been quite inconsistence in the literature [1-3] on the defect formation energies by the first principle calculation especially on oxygen vacancy (Va_O). The very first calculation performed by Zhang *et. al.* [1] showed that Va_O is a shallow donor. This calculation was later argued by Janotti *et. al.* [2], who calculated Va_O to be a deep donor with high formation energy. Janotti's results are in disagreement with the recent reported prediction by Lany *et. al.* [3]. The discrepancies are attributed to the un-certainty of "band-gap problem" and "supercell finite-size effects" [3]. Lany *et. al.* further performed the first principle calculation and simulated the equilibrium defect and electron concentrations in ZnO. In their calculation, Va_O has a metastable shallow state [4]. However, the existence of Va_O as shallow donor was supported by experiments such as deep level transient spectroscopy [5-8], Hall [9], thermally simulated current [10], electron paramagnetic resonance [11]. Thus, in this work, the formation energies of native defects obtained by Zhang *et. al.* [1] are employed in the evaluation of thermodynamic model parameters. However, our future work will examine the effect of input formation energies from first principle calculation on the predicted thermodynamic properties.

Taking the intrinsic Fermi level, E_F^* as the state of reference for charges, the formation energy of (Zn)(O)(*Va*)(*Va*) is simply the formation energy of ZnO, μ_{ZnO}^0. With the *non-degenerate* approximation of the Fermi-Dirac distribution function, the standard formation energies of electrons(e^-) and holes (h^+) are represented by $\mu_{e^-}^0$ and $\mu_{h^+}^0$, respectively and were obtained by eqns. (1) and (2) [12-13],

$$\mu_{e^-}^0 = \frac{E_g}{2} + \frac{k_0 T}{2} \ln(m_e^* / m_p^*)^{3/2} - RT \ln N_c \qquad (1)$$

$$\mu_{h^+}^0 = \frac{E_g}{2} - \frac{k_0 T}{2} \ln(m_e^* / m_p^*)^{3/2} - RT \ln N_v \qquad (2)$$

where E_g is the temperature-dependent band gap of ZnO. k_0 is Boltzmann constant. m_e^* and m_p^* are the effective electron mass and effective hole mass, respectively. N_c and N_v are the effective states (quantum limit concentrations, numbers per sublattice site) of electrons and holes at the conduction and valence band edges. The formation energies of (Zn)(O)(*Va*)(e^-), (Zn)(O)(*Va*)(h^+), $\mu_{ZnOVae^-}^0$ and $\mu_{ZnOVah^+}^0$, were defined as $\mu_{ZnO}^0 + \mu_{e^-}^0$ and $\mu_{ZnO}^0 + \mu_{h^+}^0$ corresponding to an excitation of the semiconductor to the conduction or valence band edge, respectively. The formation energies of single defects, Va_O, Zn_O, Zn_i, Va_{Zn} and O_i obtained by the first principle calculations[4] were incorporated into the model. Species whose formation energies were not calculated by the first principles calculations were derived from the reciprocal reactions. For example, defect complex (Va_{Zn}-Zn_i) is calculated by summing the Gibbs energies for single defect of Va_{Zn} and Zn_i, namely, $G(Va_{Zn}OZn_iVa) = G(Va_{Zn}OVaVa) + G(ZnOZn_iVa)$. More accurate formation energies of defects or dopants could be obtained through optimization if the

concentrations or other thermodynamic properties of defects or dopants can be precisely measured by experimental methods due to the self-consistency of thermodynamics.

The intrinsic carrier concentration calculated using the set of parameters described in the previous paragraph is shown in the solid line in Fig. 7. The dotted line is directly derived from the Fermi-Dirac function. A good consistence is established between these two methods, which indicates the feasibility of our thermodynamic model. Fig. 8. is the calculated phase diagram of ZnO. The composition axis is zoomed in to show the nonstoichiometric composition range of ZnO due to the native defects. The nonstoichiometric composition range of ZnO is totally located in the Zn-rich side and a non-stoichiometric melting point inclining to the Zn end.

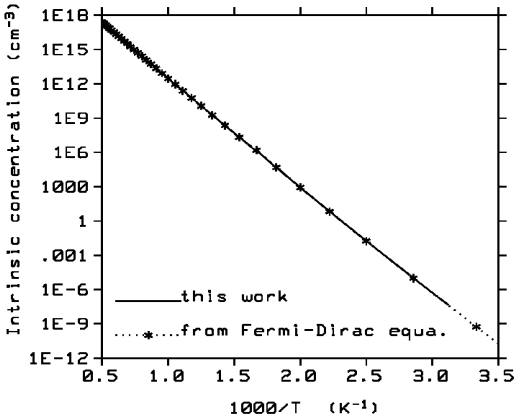

Fig. 7. Calculated intrinsic carrier concentration of ZnO

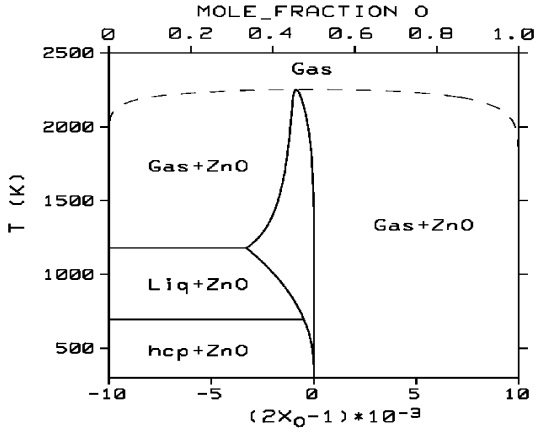

Fig. 8. Calculated phase diagram of the binary Zn-O system with P = 1 atm, Xo stands for oxygen mole fraction.

The temperature dependence of concentrations of these native defects and carriers are calculated under the Zn-rich condition (mole fraction of Zn=0.6, Fig. 9a) and the O-rich condition (mole fraction of O=0.6, Fig. 9b), respectively. It indicates that the Va_O^{+2} (a donor) is always the dominative defect at both Zn-rich and O-rich conditions. This implies that the ZnO is an intrinsically n-type semiconductor as concluded by other literatures [1,5-11]. The concentration of Va_O^{+2} is much higher at the Zn-rich condition than at the O-rich condition. The calculated concentrations of Va_{Zn} and O_i are too small and thus are not shown in the figure. The concentrations of carriers and defects increase rapidly with temperature. The carrier and native defect concentrations are determined by specific growth techniques and growth conditions. In general, the carrier concentration under Zn-rich condition is in the order of 10^{17}~10^{20} cm^{-3} and is higher than that under O-rich conditions [14]. Our calculated carrier concentration under Zn-rich condition is in the order of 10^{18}~10^{20} cm^{-3} which is in good agreement with experimental observations [14-15]. Our calculated carrier concentration for O-rich condition is also consistent with experimental values [16] For example, the ZnO annealed in O_2 (O-rich) of 800°C [16] has carrier concentration of 10^{17} cm^{-3} and our calculated value at T=1073 K is 3.2×10^{16} cm^{-3} as shown in Fig. 9(b). However, the calculated carrier concentration for O-rich is generally lower than experimental values [14-15]. Even though Va_O is dominant defect for both Zn-rich and O-rich conditions, for the Zn-rich condition, the Va_O concentration is high and the contributions from other impurity defects are negligible. On the other hand, for the O-rich conditions, the unintentional donor impurities such as Al should be taken into consideration [17] because of the overall low defect concentration of Va_O. External impurities are difficult to avoid during ZnO growth. In addition, most of ZnO with the published carrier concentration data are grown by

non-equilibrium process such as PLD process which would lead to more structural defects. The hydrothermal growth is a near-equilibrim process and it generates ZnO with much lower carrier concentration of 10^{15} cm^{-3} which is in good agreement with our calculations [8]. In addition, disagreement has been observed between this work and the first principle calculation by Lany *et. al.*[4]. The discrepancy is again attributed to the difference of the formation energies especially the Va_O. Despite all of the uncertainties mentioned above, this defect model of ZnO can intuitively exhibit the behavior of defects and carriers, and provide the information of how the growth condition affects the defect/dopant and carrier concentrations. Thus, a quantitative analysis of the doping chemistry of a specific growth process is realizable using this model by taking into account the corresponding doped species and chemical conditions. This will be our partial work in the next stage.

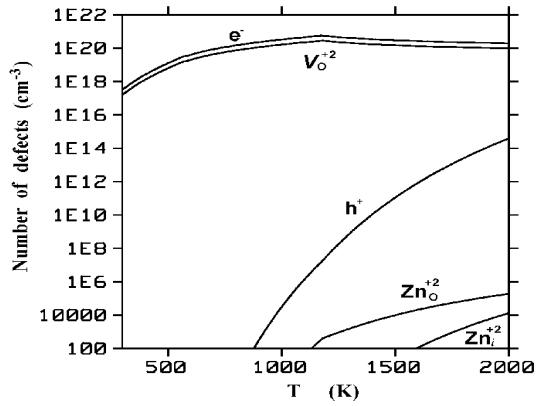

Fig. 9 (a) Calculated temperature dependency of the native defect concentrations in ZnO at the Zn-rich condition (X(Zn) = 0.6);

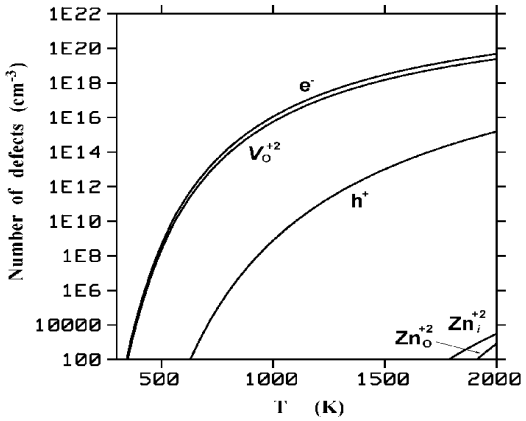

Fig.9 (b) Calculated temperature dependencies of the concentrations of defects in ZnO with P = 1 atm at the O-rich condition (X(O) = 0.6).

In conclusion, a four sublattice model is developed to provide a quantitative description of the behavior of native defects and carriers in ZnO. A nonstoichiometric composition range of ZnO due to the existence of native defects is located in the zinc rich side. ZnO is calculated to be an intrinsically *n*-type semiconductor. The predicted thermodynamic properties of ZnO as a function of input formation energies from first principle calculation will be investigated in the future.

References in this paper

[1] S. B. Zhang, S.-H. Wei, and A. Zunger, Phys. Rev. B, **63** (2001) 075205.
[2] A. Janotti and C. G. Van de Walle, Physical Review B, **76** (2007) 165202.
[3] S. Lany and A. Zunger, Physical Review B, **78** (2008) 235104.
[4] S. Lany and A. Zunger, Physical Review Letters, 98 (2007) 045501.
[5] Z.-Q. Fang, B. Claflin, D. C. Look, Y.-F. Dong and L. Brillson, J. Vac. Technol. B, **27 (3)** (2009) 1774.
[6] J. C. Simpson and J. F. Cordaro, J. Appl. Phys. **63** (1988) 1781.
[7] F. D. Auret, S. A. Goodman, M. J. Legodi, W. E. Meyer, and D. C. Look, Appl. Phys. Lett. **80** (2002) 1340.
[8] H. von Wenckstern, H. Schmidt, M. Grundmann, M. W. Allen, P. Miller, R. J. Reeve, and S. M. Durbin, Appl. Phys. Lett. **91** (2007) 022913.

[9] D. C. Look, D. C. Reynolds, J. R. Sizelove, R. L. Jones, C. W. Litton, G. Cantwell, and W. C. Harsch, Solid State Commun. **105** (1998) 399.
[10] Z.-Q. Fang, B. Claflin, D.C. Look, G.C. Farlow, J. Appl. Phys. **101** (2007) 086106.
[11] S.M. Evans, N.C. Giles, L.E. Halliburton, and L.A. Kappers, J. Appl. Phys. **103** (2008) 043710.
[12] Q. Chen and M. Hillert, J. Alloys Compd. **245** (1996) 125.
[13] J.B. Li, J.C. Tedenac, C. Li, and W-J. Zhang, CALPHAD, **27** (2003) 1.
[14] H.S. Kim, J.M. Erie, S.J. Pearton, D.P. Nortan, and F. Ren, Appl. Phys. A**. 91** (2008) 251.
[15] B.J. Jin, S.H. Bae, S.Y. Lee, and S. Im, Materials Science and Engineering, **B71** (2000) 301
[16] H.S. Kang, G.H. Kim, S.H. Lim, H. W. Chang, J. H. Kim, and S. Y. Lee, Thin Solid Films, **516** (2008), 3147.
[17] D.C. Look, Superlattices and Microstructures, **42** (2007) 284.

(5) Graduate student thesis

Wei Mu, Master's thesis title "Investigation of N single atom and diatom effect on the conductivity of ZnO:N" Miami University, Awarded in August, 2009.